Heliyon 10 (2024) e23372

Contents lists available at ScienceDirect

Heliyon

journal homepage: www.cell.com/heliyon

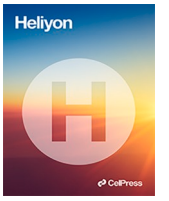

Determining optimal bead central angle by applying machine learning to wire arc additive manufacturing (WAAM)

Dong-Ook Kim [a], Choon-Man Lee [b,*], Dong-Hyeon Kim [b,**]

[a] School of Smart Manufacturing Engineering, Changwon National University, Changwon, Republic of Korea
[b] Mechatronics Research Center, Changwon National University, Changwon, Republic of Korea

ARTICLE INFO

Keywords:
Wire arc additive manufacturing (WAAM)
Machine learning (ML)
Support vector machine
Central angle

ABSTRACT

Wire arc additive manufacturing (WAAM) is being extensively used in various industrial fields. In WAAM, if a bead is deposited without considering the central angle, its shape may collapse with increasing number of layers. To address this problem, a new method for optimizing the bead geometry using a support vector machine (SVM) classifier was established in this study. The ranges of the optimal deposition conditions were determined using the SVM classifier and verified by experiments. Geometric data of deposited beads were extracted using a laser profiler, and an SVM binary classifier was used to predict suitable ranges of the deposition conditions. Data were extracted through 20 single-layer basic experiments, classification was performed based on 4°, and the appropriateness of SVM classification was found through 8 single-layer and 3 multi-layer verification experiments.

The results showed that the SVM classifier successfully selected the ranges of the optimal deposition conditions. Verification experiments revealed that the results in all cases were appropriately classified based on the boundary of the classification line. Moreover, the SVM classifier was efficient even when a small amount of input data was available. The contribution of this study is that the developed method can help build desired bead geometries in scenarios where deposition is required in the WAAM process, such as re-manufacturing. Thus, this method can be used in real-world industrial applications through further research on the bead shape with multi-layer deposition.

1. Introduction

Wire arc additive manufacturing (WAAM) is a type of direct energy deposition process for fabricating fully dense large three-dimensional (3D) near net shape metal parts, and it offers multiple advantages, such as high deposition rate and low manufacturing cost [1]. Therefore, owing to its economic benefits, WAAM has received considerable interest in several fields related to large-scale industrial production, particularly in the aerospace industry. Common arc welding technologies include gas metal arc welding (GMAW), gas tungsten arc welding (GTAW), and plasma arc welding (PAW) [2]. Fig. 1 shows the schematics of the GMAW, GTAW and PAW processes.

GMAW is a welding process where external shielding gas and consumable wires are injected. It is widely used owing to its high

* Corresponding author.
** Corresponding author.
E-mail addresses: cmlee@changwon.ac.kr (C.-M. Lee), dkim@changwon.ac.kr (D.-H. Kim).

https://doi.org/10.1016/j.heliyon.2023.e23372
Received 25 September 2023; Received in revised form 23 November 2023; Accepted 1 December 2023
Available online 7 December 2023

productivity and reliability. Cold metal transfer (CMT) is the most commonly used process in WAAM by GMAW and is a modified short-arc method because of its low heat input and high deposition rate [3] GTAW can produce high-quality welds using a separately fed wire with a nonconsumable tungsten electrode without spatter or slag. The PAW process is similar to that of GTAW, except that the PAW arc is squeezed through a torch nozzle [4]. Several studies have focused on the WAAM process. Hwang et al. [5] investigated the effects of the pressure rolling of wire arc additively manufactured IN625-SS308L bimetallic structure. Ren et al. [6] proposed a novel WAAM process to produce porous metal. The novelty is to convert harmful welding pore defects into a beneficial structure of porous metal, and then the parts can be additive manufactured layer by layer. Vora et al. [7] performed the GMAW based WAAM process for fabricating a multi-structure at optimized process parameters on SS316L using metal wire of SS316L. Gürol et al. [8] performed a comparative study on the stainless steel 316 parts manufactured by WAAM and sand casting to reveal the microstructural, mechanical, wear, and corrosion behaviors. Chen et al. [9] studied the effect of equivalent heat input on WAAM aluminum-silicon alloy. The refinement of microstructure was easily obtained by using the smaller current and voltage. Vora et al. [10] optimized the bead morphology for GMAW-based WAAM of 2.25 Cr-1.0 Mo steel using metal-cored wires. The Box–Behnken design was employed to perform the experiments with the considerations of process variables of wire feed speed, travel speed, and voltage. The bead width and the bead height were selected as the response variables. The teaching learning-based optimization algorithm was used for the optimization of the response variables. The aforementioned studies reviewed the overall aspects of WAAM research, such as material properties and path planning. Recently, with the development of various algorithms, machine learning (ML) has been increasingly applied to all types of WAAM, regardless of the material, process, and shape.

WAAM is also used to repair damaged metal parts. In this process, if the torch angle is adjusted during deposition without considering the deposition conditions, the bead shape may collapse. Therefore, when depositing on a damaged part, adjusting the angle is necessary.

This study aimed at minimizing the bead collapse in the WAAM process. To this end, the ranges of the optimal deposition conditions were determined using the ML method.

The bead central angle is typically several degrees off the vertical axis, as shown in Fig. 2. A large inclination angle can decrease the geometry accuracy.

In WAAM, if a bead is deposited without considering the central angle, its shape may collapse with increasing number of layers. A large inclination angles of the beads can cause the collapse during multi-layer deposition. To address this problem, a new method for optimizing the bead geometry using a support vector machine (SVM) classifier was established in this study.

In this study, the trends in recent studies focusing on the application of ML to WAAM were reviewed and summarized. Section 2 discusses the state-of-the-art ML applications in WAAM. Section 3 presents the newly established method for optimizing the quality of deposition by ML, which is identified as an area still lacking in research, and describes the WAAM experiments conducted to evaluate the developed method. Section 4 presents and discusses the single-layer experimental results. Subsequently, it presents the multi-layer deposition experiments and analysis performed under single-layer conditions selected based on a support vector machine (SVM) classifier. Finally, Section 5 summarizes the conclusions of the study.

2. State of the art

This section discusses the recent research on the application of ML to WAAM. The industrial use of WAAM still faces challenges such as low dimensional accuracy and layered morphologies. Resolving these problems and improving the geometric accuracy are important for appropriately manufacturing products. In addition, the mechanical properties and defects of products, such as humping, pores, and arc instability, need to be improved.

An artificial neural network (ANN) is an ML algorithm that imitates the principles and structures of a human neural network [11]. The inputs are stimulation and signal data, the threshold is a weight, and the output data are the results of the performed computations. Various studies have been conducted on the applications of ANNs to WAAM, including bead shape optimization, surface roughness

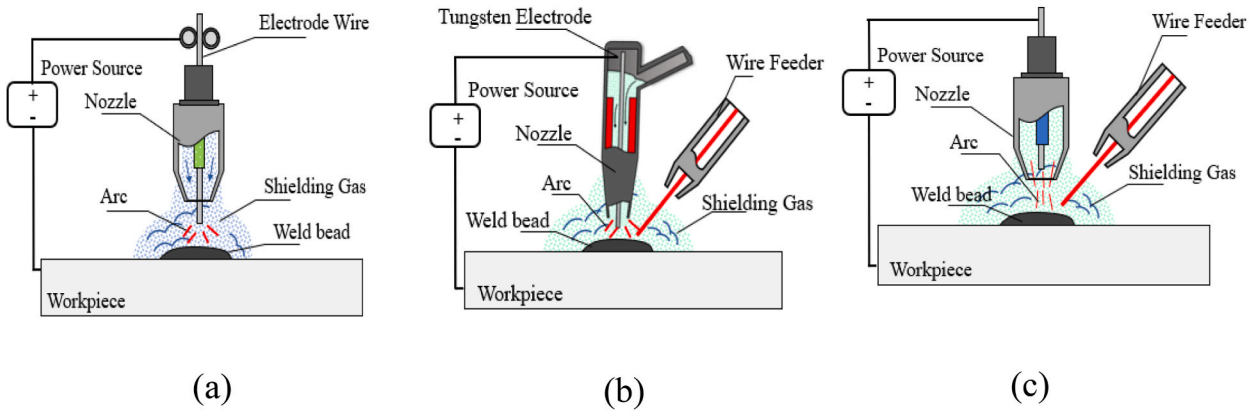

Fig. 1. Schematic of different types of arc welding techniques: (a) GMAW, (b) GTAW, and (c) PAW.

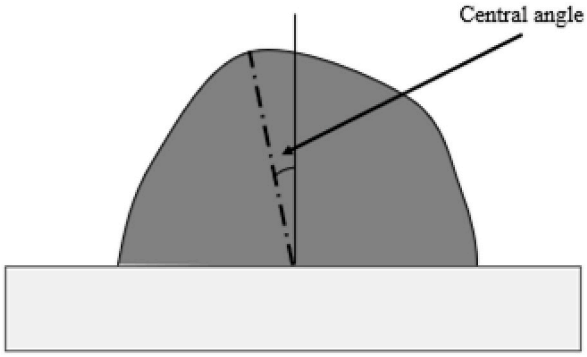

Fig. 2. Schematic of the bead central angle.

prediction, path strategy planning, and residual stress and interpass temperature prediction [12–19]. Karmuhilan and Sood [13] used a forward and reverse ANN model to predict bead geometry and welding parameters. The results showed that this method can be used to predict the process parameters of WAAM. Yaseer and Chen [18] developed random forest (RF) and multi-layer perceptron (MLP) models to predict the layer roughness when using a weaving path for WAAM. Nguyen et al. [14] introduced an advanced tool path planning strategy to fill the gap in the rib–web WAAM process. Wacker et al. [15] proposed an enhanced ANN model to predict the distortion of WAAM products and compared it with a standard ANN model. Xiao et al. [17] reported that standard methods (e.g., ANN and regression models) cannot effectively determine the optimal printable area based on a desired bead shape. Thus, a novel ML model that achieved a higher accuracy than the regression and ANN models was proposed. Wu et al. [16] analyzed residual stress data of three alloys using neural networks and an RF algorithm to predict the hierarchical effects of the influencing factors. Farias et al. [12] developed an interpass temperature prediction model for the WAAM process based on an ANN using finite element method (FEM) simulation results. Their method combined the advantages of precision and cost reduction of FEM simulations with those of fast and adaptive calculation capability of ANNs to achieve a balance between manufacturing productivity and part behavior. Yu et al. [19] developed an advanced ANN prediction model for welding reinforcement using backpropagation. The verification showed that the developed model accurately predicted welding reinforcement. Studies have also been conducted using deep neural networks, which consist of ANNs with two or more hidden layers. He et al. [20] designed a predictive network to estimate the offset of a layer during the CMT process. Welding pool images captured under seven different offset conditions were classified with an accuracy of 96.65 %.

The loss of image space information caused by their structures makes ANNs inefficient when extracting and learning features, thereby limiting their accuracy. Convolutional neural networks (CNNs) offer advantages over ANNs for solving complex tasks [21]. Therefore, many studies have focused on image processing [22–27]. Lee et al. [25] proposed a novel methodology for detecting weld

Table 1
Studies on the use of ANNs and CNNs for WAAM.

Process	Materials	ML methods	Inputs	Outputs	Ref.
GMAW	Copper coated mildsteel	ANN	Voltage, wire feed rate, welding speed	Bead geometry	[13]
GMAW	ER70S-6	ANN(RF,MLP)	Wire feed speed, travel speed, weaving wavelength, weaving amplitude	Layer roughness	[18]
GMAW	ER70S-6	ANN(bayesian)	Turning point, configurate junction	Path strategy	[14]
GMAW	ER70S-6	ANN	Amount of beads preheat temp, welding speed, wire feed speed,	Geometry and distortion prediction	[15]
GMAW	AISI420	ANN	Arc current, voltage, travel speed	Bead geometry	[17]
GMAW	IN718	ANN(RF)	Arc power, scanning speed, substrate thickness and preheat temperature,	Residual stress, delamination	[16]
GMAW	ER90S–B3	ANN	idle time, layer number	Interpass temperature	[12]
CMT	STS	ANN(Back-propagation neural networks)	Weld pool images	Weld quality	[19]
CMT	STS 316L	Deep residual network	Weld pool images	Deposited layer offset	[20]
GTAW	IN625	CNN, VGC16, VGC16-PRETR, VGC16-PRETR-FINETUNE	Weld-pool/bead images	Detection performance of weld-pool/bead	[25]
CMT	ER70S-6	CNN, GoogLeNet, VGG-16, ResNet, EfficientNet	Robot suspend, normal, humping, spattering (image)	Bead quailty	[28]
GTAW-P	STS304L	CNNs	Shapes of weld pool	Weld pool detect, weld penetration predict	[22]
GMAW	ER316L	ResNet-34, VGG-15, AlexNet, deep learning	Welding current	Layer width	[26]
GTAW	Molybdenum	MobileNetV2, DenseNet169, ResNet50V2, InceptionResNETV2	Melt pool images	Defect detection	[23]
GTAW	STS	CNN, RNN Transfer learning	Top-side view images	Weld penetration	[24]

pool and bead defects. Applying a CNN model on data collected using a high-dynamic range camera revealed that its performance was improved by image preprocessing. They also compared four types of CNN models, and the non-pretrained VGC16 wt model exhibited the best performance, with an accuracy of 0.965 (± 0.013). Xia et al. [28] conducted a study to visually monitor the defects in melt pools generated during the WAAM process. Four types of CNNs were used for anomaly detection: GoogLeNet, VGG-16, EfficientNet, and ResNet. The extracted images were classified by each network into four categories: humping, sputtering, robot suspended, and normal. The classification results showed that all models were highly accurate in classifying weld pool images, with GoogLeNET, VGG-16, EfficientNet, and ResNet achieving classification accuracies of 97.25 %, 97.15 %, 97.45 %, 97.62 %, respectively. Therefore, ResNet showed the best classification performance on weld pool images. Cheng et al. [22] proposed an innovative method for detecting the dynamic development of weld pools during the GTAW process. The CNN learning dataset included images collected using an active vision-based sensing system. Further, a model was designed to analyze the penetration state, yielding an accuracy of 97.5 % and a loss of 0.054. Wang et al. [26] established a monitoring and control system to improve the stability and accuracy of the WAAM process, and the developed closed-loop control algorithm offered a satisfactory forming accuracy by adjusting the weld width and reinforcement when fabricating thin-walled parts. Cho et al. [23] presented a real-time anomaly detection method for WAAM. Four CNN-based models were trained to detect abnormalities in melt pool image data. The performance of the four models was evaluated in terms of their classification accuracies and processing times. For all models, classification accuracies exceeding 95 % and processing times between 0.033 and 0.054 s/frame were obtained, indicating successful anomaly detection. Jiao et al. [24] applied a CNN and a residual neural network to predict weld penetration based on weld pool and arc top-side images. A passive vision system was used to simultaneously capture top- and back-side images. The top-side images were selected as the input data, and the penetration statuses were used as the labels. More than 120 experiments were conducted, and 28,494 image pairs were collected as the raw dataset, which was divided into validation, training, and testing datasets comprising 22,794, 2849, and 2851 images, respectively. The results showed that the ResNet with transfer learning and CNN models achieved welding prediction accuracies of 96.35 % and 92 %, respectively. Table 1 summarizes the studies on the use of ANN and CNN algorithms for WAAM.

Owing to the advantages of SVMs for classification, their application to WAAM for weld quality evaluation and defect detection has been studied [29–33]. Support vector regression (SVR) is a generalized type of SVM that introduces an insensitivity loss function ε-in regression analysis [34]. Some studies have used SVR algorithms to predict process parameters and surface roughness [27,35]. Huang et al. [29] used an SVM model for detecting surface defects and classified extracted topography images into normal and defect categories by converting 3D profiles into two-dimensional (2D) ones. A classification accuracy of 99.8 % was achieved by selecting features based on importance. Nalajam and Ramesh [33] compared the performances of SVM and RF classifiers for porosity detection. The pixel texture features of each image used in learning were extracted using Gabor filters. The proposed RF and SVM classifier models yielded accuracies of 99.49 % and 98.75 %, respectively. Li et al. [31] combined an SVM algorithm and an incremental learning model to detect defects, such as pores and humps. The experimental results showed that after training, the reliability of the novel system exceeded 90 % and that it was suitable for retraining to include new defects. Moinuddin et al. [32] used decision tree and nonlinear SVM classifiers to monitor the weld quality of a semi-automated GMAW process and found that both models appropriately classified weld defects. Jimi et al. [30] presented a new method based on a gray-level co-occurrence matrix for processing melt pool images. The gas flow rate in the CMT + Pulse (CMT + P) additive manufacturing process was predicted by SVM-cross-validation (SVM-CV) classification, with an accuracy of 91 %. Ding et al. [35] proposed a WAAM automated welding bead modeling system. The process parameters were predicted from overlapped distances (ODs) and bead heights (BHs) obtained from experiments using an SVR algorithm. The mean square errors of the OD and BH were 0.0474 and 0.0068, respectively, indicating high accuracy. In addition, this method could effectively reduce material waste and improve production efficiency compared with conventional weld bead methods. Xia et al. [27] used ML algorithms—adaptive neuro-fuzzy inference system (ANFIS), extreme learning machine (ELM), and SVR—to predict the surface roughness of layers deposited by WAAM. The welding speed, wire feed speed, and overlap ratio were selected as the input data, and the surface roughness was selected as the output. The ANFIS model was optimized using a genetic algorithm (GA) and particle swarm optimization (PSO). Among these methods, the GA-ANFIS achieved the best performance with an R^2 value of 0.9351, which was higher than that of the SVR model (0.862). Table 2 summarizes the studies on the use of SVM and SVR algorithms for WAAM.

In addition to the research on ANN, CNN, and SVM algorithms, studies have focused on the use of other types of ML algorithms for

Table 2
Studies on the use of SVM and SVR for WAAM.

Process	Materials	ML methods	Inputs	Outputs	Ref.
CMT	AL5087 filler	SVM	Topography image	Defect detection	[29]
CMT	AA4043	SVM, RF,	Microstructural images	Porosity detection	[33]
CMT	ER706-S	SVM	Current, voltage	Defect detection	[31]
GMAW	ER70S-6	SVM, Decision tree approach	Wire feed rate, stick out distance, travel speed, gas flow rate	Weld quality	[32]
CMT + Pulse	HCr20Ni10Mn7Mo	SVM-CV	Weld pool images	Gas flow status	[30]
CMT-P	AISI4043	SVR	OD(Overlap distance), BH(Bead height)	WFS(mm/min), TS(mm/min), IPT	[35]
GMAW	ER70S-6	ANFIS, ELM, SVR	Welding speed, WFS, overlap ratio	Surface roughness	[27]

WAAM. Reisch et al. [36] investigated anomaly detection in a multivariate time series using long short-term memory (LSTM), one-dimensional convolutional (Conv1D), and autoencoder learning models, which were adopted to avoid data labeling. To emphasize the modular concept, each model was used for current and voltage prediction and video evaluation. The proposed approach detected defects such as oxidation, polluted surfaces, and shape deviations, offering good performance using all three models. Panda et al. [37] predicted bead dimensions using various algorithms such as gene expression programming (GEP) and multi-gene genetic programming (MGGP). The peak current, travel speed, and wire feed speed were used as input parameters. The 2D and 3D geometry analyses revealed that the peak current significantly affected the BH and width. Reimann et al. [38] proposed a novel regression equation to predict $t_{8/5}$ cooling times and mechanical properties, such as hardness, tensile strength, yield strength, and elongation at break. The proposed equation achieved a high prediction accuracy, with deviations between the predicted and measured hardness, tensile strength, yield strength, and elongation at break values of only 1.2 %, 1.1 %, 0.7 %, and 2.6 %, respectively. Dharmawan et al. [39] proposed an integrated learning-correction framework based on model-based reinforcement learning to control multi-layer multi-bead deposition. The experimental results revealed that the proposed learning framework improved the surface finishing and closeness to a near net shape in the WAAM process. Lee [40] proposed a parameter optimization model using Gaussian process regression (GPR). The wire feed rate, travel speed, and interpass time output values were optimized to improve the accuracy of the deposited shape and productivity. The deposition quality was subsequently analyzed in terms of the effective area, height difference, and deposition angle, which were predicted with errors of only 4.2 %, 4.3 %, and 0.1 %, respectively, compared to the experimental values. Barrionuevo et al. [41] compared the wall widths for plasma WAAM predicted using various regression ML methods. The importance of hyper-parameter tuning was demonstrated by comparing the prediction results obtained using the lazypredict library and traditional algorithms. The latter included MLP, longitudinal SVR (LSVR), extreme gradient boosting regression (XGBR), RF regression (RFR), genetic programming (GP), GBR, adaptive boosting (AdaBoost), and decision tree regression (DTR). Thompson Martínez et al. [42] combined two ML techniques to predict weld bead geometry. First, weld bead dimensions—width, depth, and height—were obtained using a CNN-based algorithm. Subsequently, regression algorithms with good predictive performance were selected. The wire feed speed, voltage, welding velocity, un-melted wire length, and volume were used as the input. The proposed framework showed high potential for predicting and controlling the GMAW process. Oh et al. [43] predicted the deposition bead geometry in WAAM using machine learning. Le et al. [44] developed a robust surrogate model for predicting the temperature history in WAAM based on the combination of machining learning and finite element simulation. The model was built to predict the temperature history in the WAAM of single weld tracks. Sharma et al. [45] forecasted the process parameters using machine learning techniques for WAAM process. The study investigated the forward and backward correlation of data predictions of respective output and input from a machine learning perspective.

Table 3 summarizes the aforementioned studies.

While ANN and CNN consist of input, hidden, and output layers, SVM is structured around support vectors to define decision boundaries. ANN and CNN, leveraging backpropagation, exhibit robust performance on extensive datasets, albeit with potentially extended training times. In contrast, SVM operates effectively even on smaller datasets, employing support vectors to determine decision boundaries.

These differences underscore the suitability of each model for specific purposes and datasets, emphasizing the critical importance of informed model selection in research and applications.

Achieving an accurate bead geometry is important for meeting production requirements. In industrial fields where WAAM is used, deposition may be performed by adjusting the torch angle. When multiple layers are deposited, the bead shape may collapse as the deposition progresses.

Therefore, this study developed a method for optimizing the bead central angle by applying ML to the WAAM process. Geometric data of deposited beads were extracted using a laser profiler, and an effective SVM binary classifier was selected as the ML model for optimizing the bead central angle and predicting suitable ranges of the deposition conditions.

wire length, and volume were used as input. The proposed framework has a high potential for predicting and controlling the GMAW

Table 3
Studies on the use of various ML methods for WAAM.

Process	Materials	ML methods	Inputs	Outputs	Ref.
GMAW	AISI12	LSTM, Conv1d,Autoencoder	Current, voltage	Defect detection	[36]
GTAW	SA06	Gep, *m*-ggpg	Peak current, wire feed speed, and travel speed	Bead geometry	[37]
GMAW	ER70S-6	The regression equations	t8/5 cooling time and hardness, tensile strength, yield strength and elongation	Mechanical properties based on different cooling times	[38]
GMAW	ERCuNiAl	Reinforcement Learning	Torch speed(mm/s), wire feed rate (m/min)	Surface finish, bead shape	[39]
CMT	M-316L	GPR	Wire feed Rate(m/min), Travel speed(m/min) Interpass Time	Process parameters	[40]
PAW	Ti–6Al–4V	MLP,LSVR, XGBR, RFR,GPs,GBR, AdaBoost,DTR	Current, voltage, plasma gas flow rate	Layer geometry	[41]
GMAW	ER770S	Lasso regression, Ridge regression, ElasticNet regression, Least Angle Regression (LARS), Bayesian regression, SVM polynomial,SVM-RBF	Welding images	Bead geometry prediction	[42]

process. Table 3 summarizes the aforementioned studies.

Bead geometry accuracy is important for meeting production requirements. In industrial fields where WAAM is used, deposition may be performed by adjusting the torch angle. When multiple layers are deposited, the shape of the bead may collapse as the deposition progresses.

Therefore, this study proposes a method for optimizing the bead central angle by applying ML to the WAAM process. The geometric data of the deposited beads is extracted using a laser profiler and an effective SVM binary classifier is selected as the ML model for optimizing the center angle of the beads and predicting a suitable range of deposition conditions.

3. Materials and methods

3.1. Methods

ML can be classified into three categories: supervised, unsupervised, and reinforced learning. Supervised learning predicts results after learning based on labeled data. Unsupervised learning identifies hidden structures and features in unlabeled data. Reinforcement learning optimizes decision-making via feedback. Classification is a type of supervised learning that identifies the relationships between categories of raw data and determines the category of a new data point. Classification algorithms include K-nearest neighbor (KNN), decision tree, naive Bayes, and SVM. KNN determines the label of a data point by finding data close to this point among other data with various labels. A decision tree is a combination of predictable rules that represent patterns existing in data by data analysis. The naive Bayes algorithm uses probabilities to learn about events that have already occurred and predict new events. SVMs use decision boundaries to identify boundaries that classify two groups and offer excellent performance for clearly classifiable data groups. The principle of an SVM is as follows. A dataset is classified by selecting an appropriate plane. The SVM model selects a suitable hyperplane in a high-dimensional space for classifying input data. This hyperplane creates the maximum margin between the classes in the input data, representing the longest distance between the data points. The margin is the distance between the classification interface and the minus and plus planes dividing the classes. The width of the margin is $\frac{2}{\|w\|}$, where w is the vector perpendicular to the classification interface. When the margin is maximum, w is minimum and the SVM is optimized. The advantage of SVM models is that they can be constructed by regression or classification using a relatively small amount of data. Fig. 3 shows the functional diagram of an SVM.

3.2. Experimental setup

A 6-axis robot arm (IRB 6700 of ABB Ltd., Zurich, Switzerland) was used to deposit ER308L wires. A metal inert gas welding machine (TPS 500i of Fornius CO., Ltd., Pettenbach, Austria) was used to control the welding process. The shielding gas and wire were supplied by the welding machine through a welding torch. A 3D line laser scanner (Keyence GmbH., Osaka, Japan) was used to measure the bead widths and bead heights. Fig. 4 shows the experimental setup.

3.3. Materials

Stainless-steel AISI304 was used as the substrate (100 mm × 100 mm × 25 mm) in the experiments. Metal wire ER308L with a diameter of 1.2 mm was used as the deposition material. The chemical compositions of the substrate and metal wire are summarized in Table 4.

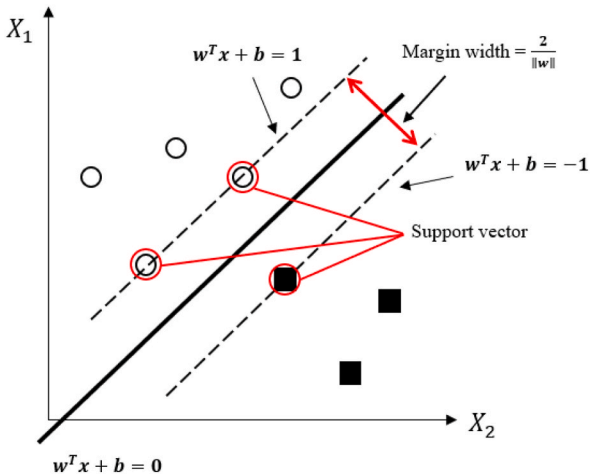

Fig. 3. Functional diagram of an SVM [46].

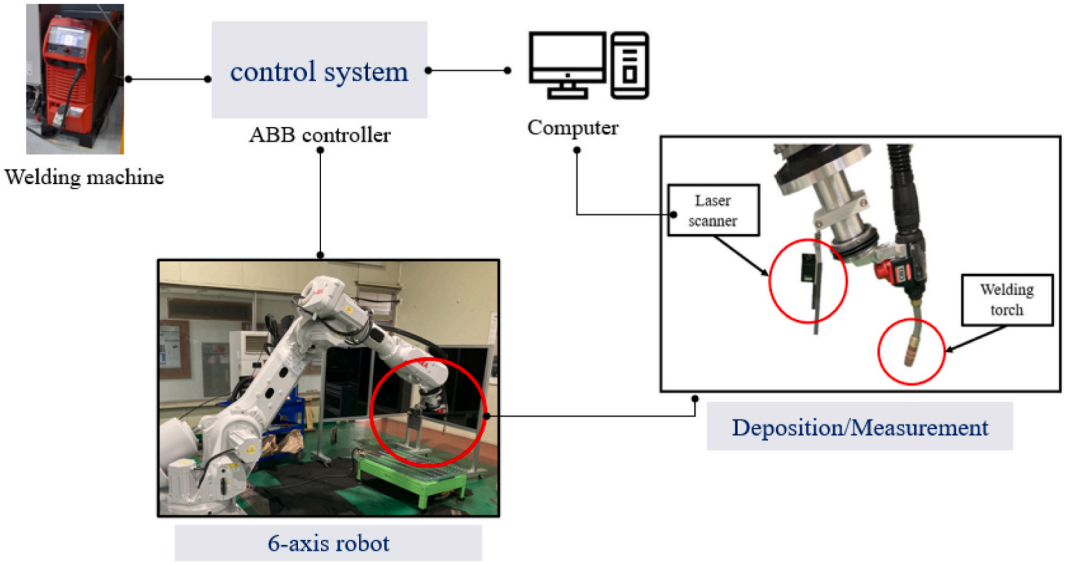

Fig. 4. Experimental setup.

3.4. Procedure

In this study, the travel speed and torch angle parameters were adjusted to select appropriate ranges for depositing beads with suitable central angles. The input process parameters are listed in Table 5. The deposition was performed with a single path of 50 mm, and the cross-sectional shapes of the beads were measured at 1.5 mm intervals using a laser profiler from 10 mm to 40 mm after deposition. The average value of 21 data per experiment was selected as the central angle of a bead based on the deposition conditions; subsequently, an SVM classification model was generated, and the optimal deposition parameters were selected. The bead central angle is the inclination angle from the vertical direction of the deposited shape. Fig. 5 shows schematics of the experiments and the measurements of the widths and heights of the specimens.

4. Results and discussion

4.1. Data collection and processing

A total of 20 experiments were conducted under different deposition conditions. Data were classified as good when the measured bead central angle was smaller than 4° and as bad otherwise. The central angle and class selection results are summarized in Table 6.

The experimental results indicate that for a given combination of the wire feed speed (WFS) and the torch angle, a high travel speed implies a strong effect of the torch angle on the bead central angle. Fig. 6 shows the classification of the results according to the deposition conditions.

4.2. Verification experiments

Based on the experiments and analysis of the results, the deposition conditions at bead central angles below 4° were collected. Subsequently, experiments were conducted to verify the classification accuracy. The verification experiments were repeated eight times, randomly selecting deposition conditions that did not overlap with those used in the experiments. In addition, 21 central angle data were extracted for each experimental case to obtain the average value. The results of the eight repetition experiments are summarized in Table 7.

The experimental results in both the good and bad regions show that the upper and lower bead central angles are smaller and larger than 4°, respectively, based on the boundary. This suggests that a simple binary classification using the SVM model is effective even when the number of samples is small.

Table 4
Chemical composition of substrate and filler (wt%).

Material	C	Mn	Cr	Ni	S	P	Cu	Nb	Ti	V	Fe
AISI 304	0.080	2.000	19.50	10.50	0.030	0.007	–	–	–	–	Bal.
ER308L	0.030	2.500	25.00	14.00	0.030	0.030	0.75	–	–	–	Bal.

Table 5
Process parameter ranges used in experiments.

Process parameter	Variables
Current (A)	130
Voltage (V)	14.1
Travel speed (mm/s)	4, 5, 6, 7
Wire feed speed (m/min)	4.8
Torch angle (°)	50, 60, 70, 80, 90
Argon gas flow (L/min)	25
Deposition length (mm)	50

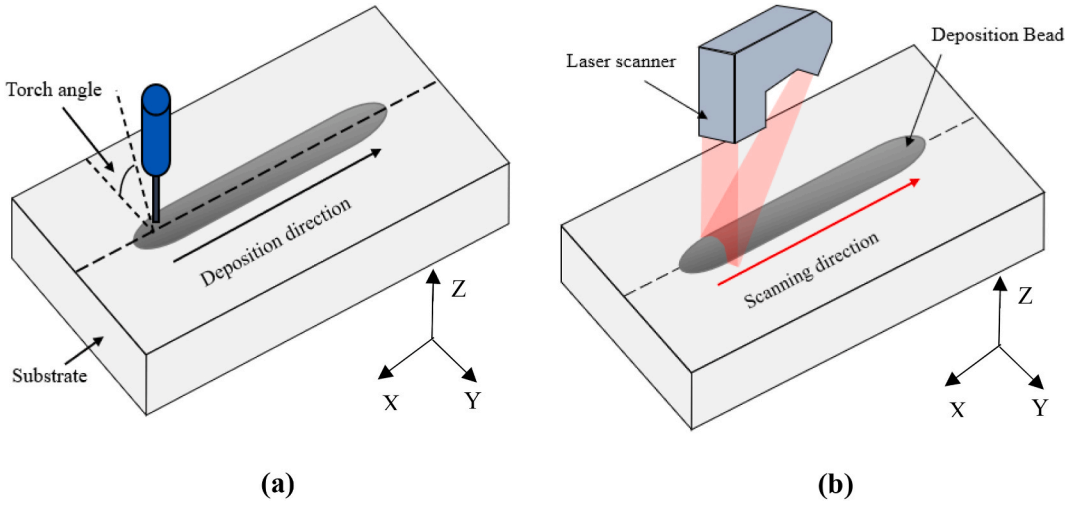

Fig. 5. Schematics of the (a) experiments and (b) measurements of the widths and heights of the 3D profiles.

Table 6
Experiment design and results.

Case	Torch angle(degree)	Travel speed(mm/s)	Central angle(°)	Class
1	50	4	11.57	Bad
2	50	5	12.61	Bad
3	50	6	16.57	Bad
4	50	7	19.54	Bad
5	60	4	7.98	Bad
6	60	5	6.31	Bad
7	60	6	10.84	Bad
8	60	7	8.43	Bad
9	70	4	3.27	Good
10	70	5	5.68	Bad
11	70	6	6.54	Bad
12	70	7	4.56	Bad
13	80	4	3.41	Good
14	80	5	2.85	Good
15	80	6	5.68	Bad
16	80	7	4.12	Bad
17	90	4	3.14	Good
18	90	5	3.58	Good
19	90	6	1.32	Good
20	90	7	0.8	Good

4.3. Multi-layer experiments using predicted conditions

Analyzing multi-layer deposition is necessary for obtaining a desired deposition shape. Therefore, based on the verification results, as presented in Section 4.2, process parameters were selected to optimize the central angle of a single-layer bead classified using the SVM. Fig. 7 shows the selected multi-layer deposition conditions used in the experiments. The process parameters are listed in Table 8. The multi-layer deposition was conducted in one direction. The direction strategy is shown in Fig. 8.

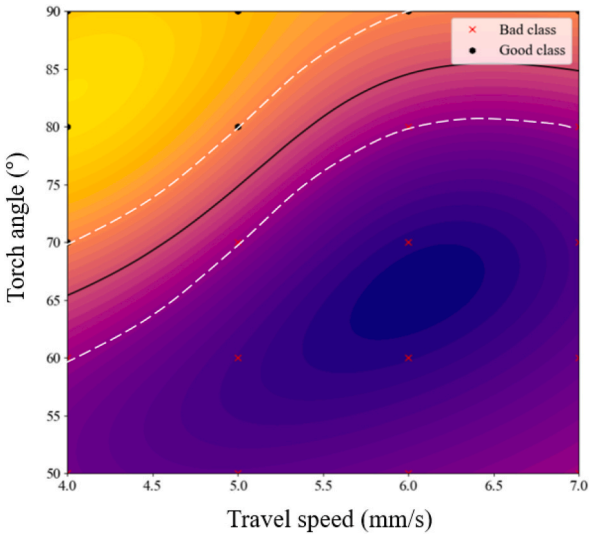

Fig. 6. Results of classification by the bead central angle.

Table 7
Results of verification experiment.

Case	Torch angle(degree)	Travel speed(mm/s)	Central angle(°)
1	75	6	8.42
2	80	5.5	5.34
3	85	7	3.91
4	90	4.5	1.47
5	55	6	13.48
6	65	5.5	7.87
7	70	6.5	6.13
8	80	4.5	3.4

The multi-layer deposition experimental results show similar trends as those of single-layer deposition; particularly, a high travel speed of the torch has a significant effect of the bead central angle. Table 9 summarizes the bead central angle results according to the conditions in each experiment. Fig. 9 shows the appearance of each five-layer deposition result obtained in the experiments. The travel speed is lowered as the torch angle increases, and a bead geometry close to the vertical may be produced.

However, the bead width or BH according to the deposition rate is not considered. If the torch angle and the travel speed are well distributed, the desired shape can be obtained.

5. Conclusion

In this study, the trends in recent research on the application of different ML methods to WAAM were examined. New methods using various ML models have been proposed to address the limitations and problems in the WAAM process.

In addition, inspired by previous studies, a new method for optimizing the bead central angle was established. The ranges of the optimal deposition conditions were determined by classifying the bead central angle according to the travel speed and the torch angle using an SVM algorithm. Through 20 experiments, bead center angle data according to deposition parameters were collected, and binary classification of good and bad data was performed based on 4°. Subsequently, it was verified that the classification was performed correctly based on the generated binary line. The results of 8 single-layer experiments showed that all classifications were performed correctly based on the boundary line.

Finally, three multi-layer deposition verification experiments were performed. It can be seen it is correctly classified according to the criteria of the binary line according to the criteria of the binary line. The conclusions are summarized as follows.

1) To investigate the suitability of the developed method, experiments were conducted under 20 different deposition conditions. The ranges of the deposition conditions were obtained using the SVM classifier after classifying the results according to the bead central angle.
2) For verification, experiments were conducted under eight randomly selected deposition conditions. The results showed that all experimental values were correctly classified based on the boundary line. This indicates that the SVM classifier is effective, even when a small amount of data is available.

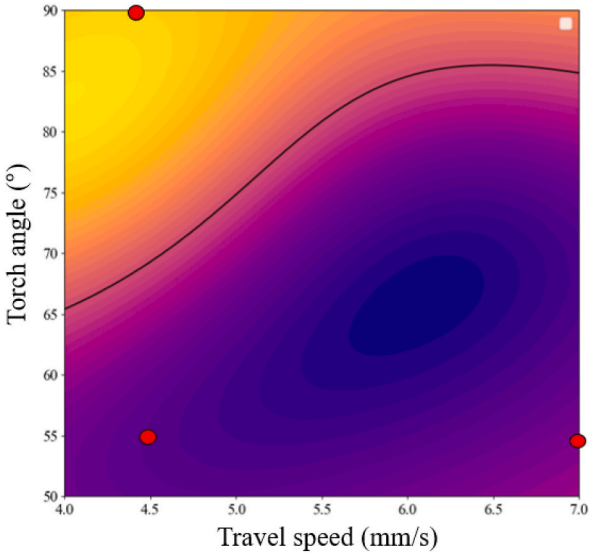

Fig. 7. Selected multi-layer deposition conditions.

Table 8
Process parameter ranges used in multi-layer experiments.

Process parameter	variables
Current (A)	130
Voltage (V)	14.1
Travel speed (mm/s)	4.5, 7
Wire feed speed (m/min)	4.8
Torch angle (°)	55, 90
Argon gas flow (L/min)	25
Deposition length (mm)	50
Idle time (min)	10
Layer number (n)	5
Contact tip with distance (mm)	15

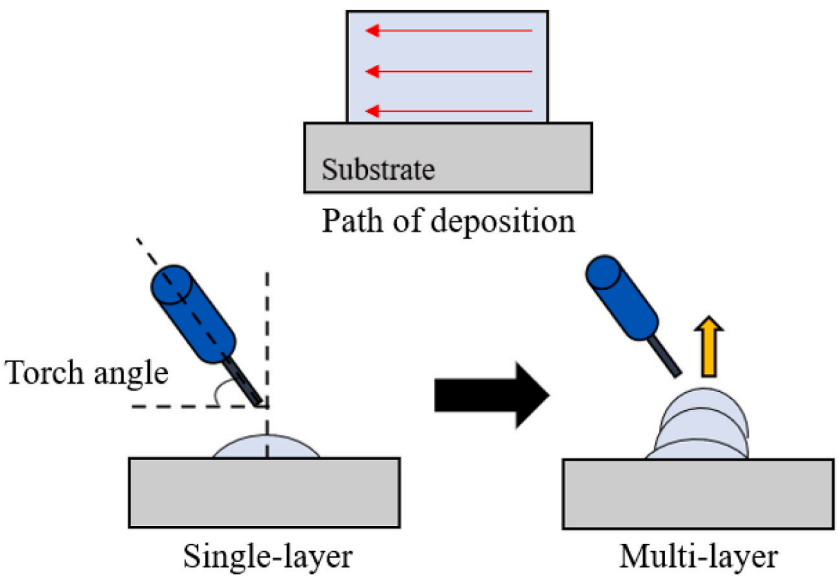

Fig. 8. Direction strategy of the multi-layer deposition.

Table 9
Results of multi-layer central angle.

Case	Torch angle(degree)	Travel speed(mm/s)	Central angle(°)	Results
a	55	7	17.61	Bad
b	55	4.5	6.86	Bad
c	90	4.5	1.72	Good

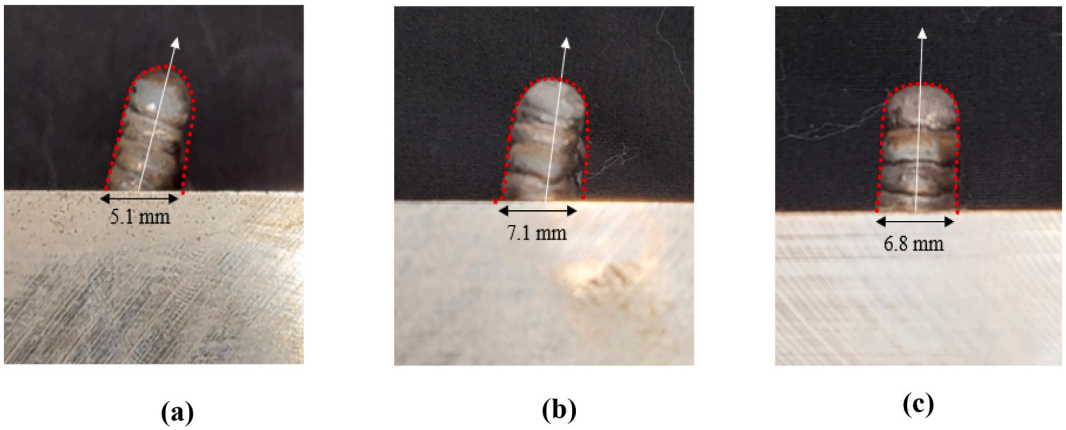

Fig. 9. Results of the multi-layer deposition experiments.

3) Multi-layer deposition experiments were performed using the process parameters selected by the SVM classification. The experimental results showed that the performance of the SVM classifier according to the angle and travel speed of the torch was suitable for both single-layer and multi-layer deposition.

Geometry data extracted from single-layer deposition by WAAM were selected to optimize the bead central angle using the SVM, and the results were successfully used for multi-layer deposition. However, the width and height of the bead shape according to the deposition conditions were not considered. Thus, the applicability of the established method to industrial applications is limited. To apply the method proposed in this study to the actual industry, multivariate analysis should be performed in consideration of current, voltage, process method, etc. A clustering method that groups similar results from multiple variables or a dimension reduction method that can effectively represent a given set of variables could be used. Therefore, further research on the bead central angle is required to improve the geometrical accuracy of the products manufactured by WAAM. Future work will focus on studying the bead central angle considering various deposition conditions.

Data availability

Data will be made available on request.

CRediT authorship contribution statement

Dong-Ook Kim: Writing – original draft, Validation, Investigation, Data curation, Conceptualization. **Choon-Man Lee:** Project administration, Funding acquisition. **Dong-Hyeon Kim:** Writing – review & editing, Visualization, Validation, Supervision, Investigation, Conceptualization.

Declaration of competing interest

The authors declare that they have no known competing financial interests or personal relationships that could have appeared to influence the work reported in this paper.

Acknowledgment

This work was supported by the National Research Foundation of Korea (NRF) grant funded by the Korea government (MSIT) (No. 2022R1A2B5B0300188412)

Nomenclature

LIST OF ACRONYMS

Abbreviation	*Description*
AM	Additive manufacturing
PBF	Powder bed fusion
DED	Directed energy deposition
WAAM	Wire arc additive manufacturing
MIG	Metal inert gas
CMT	Cold metal transfer
ML	Machine learning
SVM	Support vector machine
ANN	Artificial neural network
CNN	Convolutional neural network

References

[1] F. Wang, S. Williams, P. Colegrove, A.A. Antonysamy, Microstructure and mechanical properties of wire and arc additive manufactured Ti-6Al-4V, Metall Mater Trans A-Phys Metall Mater Sci 44 (2013).
[2] C. Xia, Z. Pan, J. Polden, H. Li, Y. Xu, S. Chen, Y. Zhang, A review on wire arc additive manufacturing: monitoring, control and a framework of automated system, J. Manuf. Syst. 57 (2020).
[3] Z. Pan, D. Ding, B. Wu, D. Cuiuri, H. Li, J. Norrish, Arc welding processes for additive manufacturing: a review, Transactions on Intelligent Welding Manufacturing 2 (2018).
[4] Y. Li, C. Su, J. Zhu, Comprehensive review of wire arc additive manufacturing: hardware system, physical process, monitoring, property characterization, application and future prospect, Results Eng 13 (2022).
[5] Y.H. Hwang, C.M. Lee, D.H. Kim, The effects of the variable-pressure rolling of a wire-arc additively manufactured Inconel 625-SS308L bimetallic structure, Appl. Sci. 13 (2023).
[6] D. Ren, X. Ba, Z. Zhang, Z. Zhang, K. Zhao, L. Liu, Wire arc additive manufacturing of porous metal using welding pore defects, Mater. Des. 233 (2023).
[7] J. Vora, H. Parmar, R. Chaudhari, S. Khanna, M. Doshi, V. Patel, Experimental investigations on mechanical properties of multi-layered structure fabricated by GMAW-based WAAM of SS316L, J. Mater. Res. Technol. 20 (2022).
[8] U. Gürol, E. Kocaman, S. Dilibal, M. Koçak, A comparative study on the microstructure, mechanical properties, wear and corrosion behaviors of SS 316 austenitic stainless steels manufactured by casting and WAAM technologies, CIRP J. Manuf. Sci. Technol. 47 (2023).
[9] C. Chen, G. Sun, W. Du, J. Liu, H. Zhang, Effect of equivalent heat input on WAAM Al-Si alloy, Int. J. Mech. Sci. 238 (2023).
[10] J. Vora, N. Parikh, R. Chaudhari, V.K. Patel, H. Paramar, D.Y. Pimenov, K. Giasin, Optimization of bead morphology for GMAW-based wire-arc additive manufacturing of 2.25 Cr-1.0 Mo steel using metal-cored wires, Appl. Sci. 12 (2022).
[11] J. Zupan, Introduction to artificial neural network (ANN) methods : what they are and how to use them, Acta Chim. Slov. 41 (1994).
[12] F.W.C. Farias, J. da Cruz Payão Filho, V.H.P. Moraes e Oliveira, Prediction of the interpass temperature of a wire arc additive manufactured wall: FEM simulations and artificial neural network, Addit. Manuf. 48 (2021).
[13] M. Karmuhilan, A.K. Sood, Intelligent process model for bead geometry prediction in WAAM, Mater. Today: Proc. 5 (2018).
[14] L. Nguyen, J. Buhl, M. Bambach, Continuous Eulerian tool path strategies for wire-arc additive manufacturing of rib-web structures with machine-learning-based adaptive void filling, Addit. Manuf. 35 (2020).
[15] C. Wacker, M. Köhler, M. David, F. Aschersleben, F. Gabriel, J. Hensel, K. Dilger, K. Dröder, Geometry and distortion prediction of multiple layers for wire arc additive manufacturing with artificial neural networks, Appl. Sci. 11 (2021).
[16] Q. Wu, T. Mukherjee, A. De, T. DebRoy, Residual stresses in wire-arc additive manufacturing – hierarchy of influential variables, Addit. Manuf. 35 (2020).
[17] X. Xiao, C. Waddell, C. Hamilton, H. Xiao, Quality prediction and control in wire arc additive manufacturing via novel machine learning framework, Micromachines 13 (2022).
[18] A. Yaseer, H. Chen, Machine learning based layer roughness modeling in robotic additive manufacturing, J. Manuf. Process. 70 (2021).
[19] R. Yu, Z. Zhao, L. Bai, J. Han, Prediction of weld reinforcement based on vision sensing in GMA additive manufacturing process, Metals 10 (2020).
[20] H. He, J. Lu, Y. Zhang, J. Han, Z. Zhao, Quantitative prediction of additive manufacturing deposited layer offset based on passive visual imaging and deep residual network, J. Manuf. Process. 72 (2021).
[21] S. Albawi, T.A. Mohammed, S. Al-Zawi, Understanding of a convolutional neural network, in: Proceedings of 2017 International Conference on Engineering and Technology, 2018.
[22] Y. Cheng, Q. Wang, W. Jiao, R. Yu, S. Chen, Y.M. Zhang, J. Xiao, Detecting dynamic development of weld pool using machine learning from innovative composite images for adaptive welding, J. Manuf. Process. 56 (2020).
[23] H.W. Cho, S.J. Shin, G.J. Seo, D.B. Kim, D.H. Lee, Real-time anomaly detection using convolutional neural network in wire arc additive manufacturing: molybdenum material, J. Mater. Process. Technol. 302 (2022).
[24] W. Jiao, Q. Wang, Y. Cheng, Y.M. Zhang, End-to-end prediction of weld penetration: a deep learning and transfer learning based method, J. Manuf. Process. 63 (2021).
[25] C. Lee, G. Seo, D. Kim, M. Kim, J.H. Shin, Development of defect detection ai model for wire + arc additive manufacturing using high dynamic range images, Appl. Sci. 11 (2021).
[26] Y. Wang, X. Xu, Z. Zhao, W. Deng, J. Han, L. Bai, X. Liang, J. Yao, Coordinated monitoring and control method of deposited layer width and reinforcement in WAAM process, J. Manuf. Process. 71 (2021).
[27] C. Xia, Z. Pan, J. Polden, H. Li, Y. Xu, S. Chen, Modelling and prediction of surface roughness in wire arc additive manufacturing using machine learning, J. Intell. Manuf. 33 (2021).
[28] C. Xia, Z. Pan, Y. Li, H. Li, Vision-based melt pool monitoring for wire-arc additive manufacturing using deep learning method, Int. J. Adv. Manuf. Technol. 120 (2022).
[29] C. Huang, G. Wang, H. Song, R. Li, H. Zhang, Rapid surface defects detection in wire and arc additive manufacturing based on laser profilometer, Measurement 189 (2022).
[30] F. Jimi, W. Kehong, Y. Dongqing, H. Yong, Gas flow status analysis in CMT+P additive manufacturing based on texture features of molten pool images, Optik 179 (2019).

[31] Y. Li, J. Polden, Z. Pan, J. Cui, C. Xia, F. He, H. Mu, H. Li, L. Wang, A defect detection system for wire arc additive manufacturing using incremental learning, J Ind Inf Integr 27 (2022).
[32] S.Q. Moinuddin, S.S. Hameed, A.K. Dewangan, K. Ramesh Kumar, A. Shanta Kumari, A study on weld defects classification in gas metal arc welding process using machine learning techniques, Mater. Today: Proc. 43 (2020).
[33] P.K. Nalajam, V. Ramesh, Microstructural porosity segmentation using machine learning techniques in wire-based direct energy deposition of AA6061, Micron 151 (2021).
[34] R.J. Kuo, P.S. Li, Taiwanese export trade forecasting using firefly algorithm based K-means algorithm and SVR with wavelet transform, Comput. Ind. Eng. 99 (2016).
[35] D. Ding, F. He, L. Yuan, Z. Pan, L. Wang, M. Ros, The first step towards intelligent wire arc additive manufacturing: an automatic bead modelling system using machine learning through industrial information integration, J Ind Inf Integr 23 (2021).
[36] R. Reisch, T. Hauser, B. Lutz, M. Pantano, T. Kamps, A. Knoll, Distance-based multivariate anomaly detection in wire arc additive manufacturing, in: 19th IEEE International Conference on Machine Learning and Applications (ICMLA), 2020.
[37] B. Panda, K. Shankhwar, A. Garg, M.M. Savalani, Evaluation of genetic programming-based models for simulating bead dimensions in wire and arc additive manufacturing, J. Intell. Manuf. 30 (2019).
[38] J. Reimann, S. Hammer, P. Henckell, M. Rohe, Y. Ali, A. Rauch, J. Hildebrand, J.P. Bergmann, Directed energy deposition-arc (Ded-arc) and numerical welding simulation as a hybrid data source for future machine learning applications, Appl. Sci. 11 (2021).
[39] A.G. Dharmawan, Y. Xiong, S. Foong, G.S. Soh, A model-based reinforcement learning and correction framework for process control of robotic wire arc additive manufacturing, in: IEEE International Conference on Robotics and Automation (ICRA), 2020.
[40] S.H. Lee, Optimization of cold metal transfer-based wire arc additive manufacturing processes using Gaussian process regression, Metals 10 (2020).
[41] G.O. Barrionuevo, S. Rios, S.W. Williams, J.A. Ramos-Grez, Comparative evaluation of machine learning regressors for the layer geometry prediction in wire arc additive manufacturing, in: IEEE 12th International Conference on Mechanical and Intelligent Manufacturing Technologies (ICMIMT), 2021.
[42] R. Thompson Martínez, G. Alvarez Bestard, A. Martins Almeida Silva, S.C. Absi Alfaro, Analysis of GMAW process with deep learning and machine learning techniques, J. Manuf. Process. 62 (2021).
[43] W.J. Oh, C.M. Lee, D.H. Kim, Prediction of deposition bead geometry in wire arc additive manufacturing using machine learning, J. Mater. Res. Technol. 20 (2022).
[44] V.T. Le, M.C. Bui, T.Q.D. Pham, H.S. Tran, X.V. Tran, Efficient prediction of thermal history in wire and arc additive manufacturing combining machine learning and numerical simulation, Int. J. Adv. Manuf. Technol. 126 (2023).
[45] R. Sharma, A.R. Paul, M. Mukherjee, S.R.K. Vadali, R.K. Singh, A.K. Sharma, Forecasting of process parameters using machine learning techniques for wire arc additive manufacturing process, Mater. Today: Proc. 80 (2023).
[46] J.S. Lim, W.J. Oh, C.M. Lee, D.H. Kim, Selection of effective manufacturing conditions for directed energy deposition process using machine learning methods, Sci. Rep. 11 (2021).